Time-Varying Ankle Mechanical Impedance During Human Locomotion

Hyunglae Lee, *Member, IEEE*, and Neville Hogan

***Abstract*—In human locomotion, we continuously modulate joint mechanical impedance of the lower limb (hip, knee, and ankle) either voluntarily or reflexively to accommodate environmental changes and maintain stable interaction. Ankle mechanical impedance plays a pivotal role at the interface between the neuro-mechanical system and the physical world. This paper reports, for the first time, a characterization of human ankle mechanical impedance in two degrees-of-freedom simultaneously as it varies with time during walking. Ensemble-based linear time-varying system identification methods implemented with a wearable ankle robot, Anklebot, enabled reliable estimation of ankle mechanical impedance from the pre-swing phase through the entire swing phase to the early-stance phase. This included heel-strike and toe-off, key events in the transition from the swing to stance phase or vice versa. Time-varying ankle mechanical impedance was accurately approximated by a second order model consisting of inertia, viscosity, and stiffness in both inversion-eversion and dorsiflexion-plantarflexion directions, as observed in our previous steady-state dynamic studies. We found that viscosity and stiffness of the ankle significantly decreased at the end of the stance phase before toe-off, remained relatively constant across the swing phase, and increased around heel-strike. Closer investigation around heel-strike revealed that viscosity and stiffness in both planes increased before heel-strike occurred. This finding is important evidence of "pretuning" by the central nervous system. In addition, viscosity and stiffness were greater in the sagittal plane than in the frontal plane across all subgait phases, except the early stance phase. Comparison with previous studies and implications for clinical study of neurologically impaired patients are provided.**

***Index Terms*—Ankle impedance, ankle joint, ankle joint stiffness, ankle stiffness, human ankle, time-varying impedance.**

I. Introduction

THE human ankle plays one of the most important roles in human locomotion at the interface between the neuro-mechanical system and the physical world to accommodate environmental changes and enable natural physical interaction [1], [2]. During locomotion, we continuously modulate ankle mechanical impedance[1] either voluntarily or reflexively to achieve important lower-extremity functions, such as shock absorption, postural stabilization, propulsion, and smooth transition from stance to swing, and vice versa.

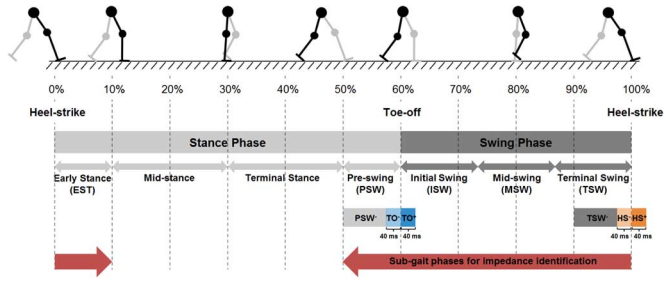

Fig. 1. Subgait phases for impedance identification. Impedance was identified in five subgait phases: pre-swing (PSW), initial swing (ISW), mid-swing (MSW), terminal swing (TSW), and early stance (EST). Time periods for closer examination around heel-strike (HS) and toe-off (TO) are illustrated.

While much has been learned about ankle impedance in steady-state (stationary) conditions [3]–[5], little is known about how ankle impedance is modulated in more general functional situations, mainly due to a lack of tools that can reliably be used for that purpose. Although a few studies have reported time-varying behavior of human ankle impedance in simulations [6], [7] or imposed movement conditions [8], [9], to the best of our knowledge, only one study directly measured ankle impedance during human walking [10]. A robotic platform was used in that study to apply angular perturbations to the ankle during mid-stance and terminal stance (Fig. 1), and ankle viscosity and stiffness were estimated in the sagittal plane between 13% and 63% of stance. Although the importance of this work overcoming the limitation of previous quasi-stiffness measurements in a traditional gait lab setting was emphasized [11], identification was limited to the period when the foot was flat to the ground and to a single degree of freedom (DOF). We may better understand human locomotion if ankle impedance in other subphases of the gait cycle is identified in multiple DOF and especially around heel-strike and toe-off where transition occurs from swing to stance or vice versa.

In this study, a wearable ankle robot, Anklebot, and modified linear time-varying (LTV) ensemble-based system identification methods were used to characterize ankle impedance from pre-swing through swing to early stance, complementing the previous work [10]. We also aimed to identify time-varying ankle impedance in 2 DOFs simultaneously, both in the sagittal and frontal planes. In the following sections, the experimental setup and protocol are described, modifications of standard LTV ensemble-based system identification methods to overcome their limitation in this application are detailed, and characterization results from young healthy subjects are provided.

Manuscript received March 04, 2014; revised June 29, 2014; accepted August 06, 2014. Date of publication August 15, 2014; date of current version September 03, 2015. The work of H. Lee was supported by a Samsung Scholarship. This work was supported by Toyota Motor Corporation's Partner Robot Division.

H. Lee was with the Department of Mechanical Engineering, Massachusetts Institute of Technology, Cambridge, MA 02139 USA. He is now with the Sensory Motor Performance Program, Rehabilitation Institute of Chicago, Chicago, IL 60611 USA (e-mail: hyunglae@alum.mit.edu).

N. Hogan is with the Mechanical Engineering Department, and Brain and Cognitive Science Department, Massachusetts Institute of Technology, Cambridge, MA 02139 USA (e-mail: neville@mit.edu).

Color versions of one or more of the figures in this paper are available online at http://ieeexplore.ieee.org.

Digital Object Identifier 10.1109/TNSRE.2014.2346927

[1]For brevity, we often omit the "mechanical" prefix.

Fig. 2. Experimental setup. Left: Anklebot connected to the custom designed shoe and the knee brace and right: Anklebot setup for walking on a treadmill.

II. Methods

A. Experimental Setup

A wearable ankle robot, Anklebot, was used to identify time-varying ankle impedance in 2 DOFs during walking on a treadmill. It is highly back-drivable with very low intrinsic mechanical impedance, and most of its mass is concentrated at the knee, not the shank or ankle (the total mass of the robot is about 3.6 kg). One recent work reported that the effect of unilateral loading due to the Anklebot on normal human walking is minimal [12]. A proper size of knee brace was selected for each subject and tightly attached to the leg with multiple Velcro straps, covering between the belly of calf muscles and approximately the middle part of thigh muscles. A proper shoe size was chosen for each subject and the foot was securely fastened with shoe laces and a wide Velcro strap over them. The body of the robot was mounted to the knee brace and end-effectors of the robot were connected to a rigid U-shaped bracket attached to the bottom of a custom designed shoe (Fig. 2 left). A shoulder strap, running up over the shoulder and neck, was also connected to the upper part of the knee brace to support the weight of the robot (Fig. 2 right). Each motor of the Anklebot (Kollmorgen RBE(H) 00714) was operated under current control and torques were reliably estimated from motor currents; the accuracy of torque estimates were verified in our previous studies (resolution of 2.6×10^{-6} Nm) [13], [14]. A linear drive (Rohlix; backlash less than 2.6×10^{-5} m) transformed torques and angular displacements of each motor to forces and linear displacements in actuator coordinates. Angular displacements and torques at the ankle in joint coordinates, defined by inversion-eversion (IE) and dorsi-plantar flexion (DP) directions, were then obtained through a nonlinear kinematic transformation [15], and recorded at 500 Hz using a digital to analog converter with 16 bit resolution (United Electronic Industries PD2-AO-8/16).

Single differential surface electromyographic (EMG) sensors (Myomonitor IV, DELSYS) were used to record muscle activity from four major ankle muscles: *tibialis anterior* (TA), *soleus* (SOL), *gastrocnemius* (GAS), and *peroneus longus* (PL). A ground electrode was placed over the patella. EMG signals were band-pass filtered (20∼450 Hz), sampled at 1 kHz, and their amplitudes were estimated using a root-mean-square average with a moving window of 200 ms after removing the dc bias offsets.

Two foot switches (force sensitive resistor membrane with bandwidth 0∼500 Hz, DELSYS) were attached to the heel and toe of the foot (Anklebot side) to detect the moment of heel-strike and toe-off events, from which the stance and swing phases of the gait were defined.

B. Experimental Protocol

Thirteen able-bodied young male subjects (all right-footed) with no reported history of neuromuscular or biomechanical disorders volunteered to participate in this study. Subjects were between the ages of 22–36 [mean (SD): 29.2 (3.7)], heights of 1.70 m–1.90 m [176.9 (5.8)], and weights 57.0 kg–90.0 kg [71.7 (9.3)]. Following procedures preapproved by MIT's institutional review board, the Committee on the Use of Humans as Experimental Subjects, informed consent was obtained from all subjects.

First, the maximum voluntary contraction (MVC) of each muscle was measured following procedures in [16], which was used as a reference to normalize EMG amplitudes. Next, subjects walked on a treadmill with the Anklebot for a few minutes but without actuation, to familiarize themselves with the experimental setup. After a few minutes of walking, subjects were asked to select their own preferred walking speed without seeing the speed indicator, so that they could walk comfortably with the added mass of the Anklebot for the duration of the experiment.

In a main experiment, a neutral position of the ankle in 2 DOFs was first measured while subjects stood upright, and subjects were instructed to walk on a treadmill with their selected preferred walking speed. After one minute of walking without actuation of the robot, mild random torque perturbations were applied to the ankle for the next 13 minutes; independent band-limited white noise with stop frequency 100 Hz was applied to each actuator to produce random torque perturbations at the ankle joint in 2 DOFs. In addition, to prevent excessive deviations from the nominal trajectory of the ankle during walking due to perturbations, the proportional gain of the controller for each actuator was set as 500 N/m [17]. The magnitude of perturbation was selected strong enough to perturb the ankle from pre-swing to early stance, but low enough not to disturb normal walking. The peak-to-peak values of the applied torques were ± 5.3 Nm/rad and ± 7.7 Nm/rad for IE and DP, respectively. Details of the controller are in [17].

Besides the main experiment, an additional study was performed to investigate the effect of random perturbations on muscle activity. A separate group of ten healthy subjects were recruited (age 18 to 24; height 1.60 m to 1.90 m; and weight 47.7 kg to 81.8 kg), who also gave written informed consent. The same experimental setup as in the main experiment was used, and subjects walked on a treadmill at their own preferred walking speed for 10 minutes, but perturbations were turned on and off every 30 seconds, from which two sets of EMG amplitudes, with and without perturbations, were compared.

C. Modified Linear Time-Varying Ensemble-Based System Identification

Human walking consists of repetitive and periodic events, often described as a gait cycle. The gait cycle begins with heel-strike of one foot, proceeds through stance and swing, and ends with another heel-strike of the same foot (Fig. 1). Limb kinematics and dynamics change within a gait cycle, but stereotypical patterns are relatively well maintained over multiple gait cycles [1]. To investigate changes of ankle impedance at each stage of the gait cycle, a time-varying system identification method is required. Among several different time-varying system identification methods, such as a time-frequency methods [18], [19], temporal expansion methods [20], [21], regressive techniques [22], [23], and ensemble-based methods [6], the ensemble-based method is well suited for this study; this method is especially efficient when multiple ensembles of input–output realizations are available as in this study. It is very robust to noisy measurements due to its averaging nature, requires no *a priori* knowledge of the structure of the system to be identified, and can capture fast time-varying behavior of the system [9].

The ensemble-based method hinges on the correlation approach presented in [6], which requires one basic assumption: that every realization experiences the same underlying time-varying behavior. A brief explanation is described as follows. For each time step i, the relationship between noise-free inputs $(u_r(i))$ and the corresponding noisy outputs $(z_r(i) = y_r(i) + n_r(i)$, where $y_r(i)$ is true output and $n_r(i)$ is additive white noise) for the rth realization of the ensemble data, can be represented as a discrete convolution equation

$$z_r(i) = \Delta t \sum_{j=0}^{M} \hat{h}(i,j) u_r(i-j) \tag{1}$$

where $\hat{h}(i,j)$ is an impulse response function (IRF) estimate with a finite lag length $L = M + 1$ ($\hat{h}(i,j) = 0$ for $j > M$, j is lag index). The lag length L was selected long enough for the IRF estimate to settle down close to zero. In this study, u_r and z_r correspond to torque inputs from the robot in joint coordinates (either IE or DP) and measure of angular displacements at the joint, respectively. By multiplying both sides of (1) with $u_r(i-k)$ and summing over all realizations and dividing them by the number of realizations (R), a Wiener-Hopf equation was obtained

$$\frac{1}{R}\sum_{r=1}^{R} z_r(i)u_r(i-k) = \Delta t \sum_{j=0}^{M} \hat{h}(i,j)\frac{1}{R}\sum_{r=1}^{R} u_r(i-j)u_r(i-k). \tag{2}$$

Thus, to identify the system dynamics at a specific time i, the input–output relation was evaluated using data across realizations (R) as well as across time (M). Equation (2) can be written simply as (3) with an input–output cross-correlation function estimate $(\hat{\phi}_{zu})$ at time i and $i-k$, and an input auto-correlation function estimate $(\hat{\phi}_{uu})$ at time $i-k$ and $i-j$

$$\hat{\phi}_{zu}(i,-k) = \Delta t \sum_{j=0}^{M} \hat{h}(i,j)\hat{\phi}_{uu}(i-k, k-j). \tag{3}$$

By changing the lag index k from 0 to M, a matrix (4) can be obtained, where $\hat{\mathbf{\Phi}}_{uu}(i)$ is an $L \times L$ matrix and $\hat{\mathbf{\Phi}}_{zu}(i)$ are $L \times 1$ vectors, and the IRF estimate $(\hat{\mathbf{h}}(i))$ is obtained from an inverse matrix operation

$$\hat{\mathbf{\Phi}}_{zu}(i) = \Delta t \hat{\mathbf{\Phi}}_{uu}(i)\hat{\mathbf{h}}(i) \tag{4}$$

$$\hat{\mathbf{h}}(i) = \frac{1}{\Delta t}\hat{\mathbf{\Phi}}_{uu}(i)^{-1}\hat{\mathbf{\Phi}}_{zu}(i). \tag{5}$$

As mentioned earlier, this method is valid only when the system undergoes the same time-varying behavior across each realization of the ensemble set. Although this assumption may be valid for simulations or strictly limited experiment conditions, it does not hold for practical applications such as human walking; even when the walking is constrained at a fixed speed on a treadmill, spatio-temporal gait parameters are not exactly same for each gait cycle, preventing direct application of the original ensemble-based method. To address this issue, two simple solutions were explored in this study: time-scaling (normalization) of realizations and rejection of highly variable realizations.

First, two ensemble sets, one for stance and the other for swing, were constructed based on heel-strike and toe-off identified by foot switch data. Then, all realizations of the stance ensemble set were normalized to the mean stance duration, and the swing set to the mean swing duration. To check the validity of this approach, the effect of time-scaling (normalization) on the distortion of impedance estimation was investigated in simulation (see Section IV).

Second, highly variable realizations were discarded based on three criteria: temporal—deviation of stance (or swing) duration from the mean of all realizations; spatial—the mean deviation of the DP angle from the nominal DP angle over the gait cycle; and neurophysiological—deviation of the EMG level of TA and *triceps surae* (the combination of SOL and GAS) from the corresponding nominal activation profile. For each of these selection criteria, the outermost 5% of all realizations were discarded.

D. Time-Varying Ankle Parameters in Joint Coordinates

With application of the modified LTV ensemble-based method described previously, time-varying ankle dynamics in joint coordinates (IE and DP) can be obtained as a set of IRF estimates. One important thing to note is that proper inputs $(u_r(i))$ and outputs $(z_r(i))$ should be defined for the IRF calculation. Output sensor measurements $(z_m(i))$ contain two components: one as a result of the input torque perturbations and the other one simply due to walking, which we called a nominal trajectory $(z_0(i))$. To identify ankle dynamics during walking, we need to relate input $(u_r(i))$ to the displacement outputs $(z_r(i))$ purely due to input torque perturbations. The outputs for system identification $z_r(i)$ were obtained by subtracting $z_0(i)$ from $z_m(i)$, where $z_0(i)$ was the average of all selected realizations. The averaging process is valid since averaging of a large number of realizations (over 400) minimized the effect of random perturbations.

The IRF estimates $(\hat{\mathbf{h}}(i))$ were obtained at each time step (at 2-ms intervals since the measurement rate was 500 Hz), and smoothed IRF estimates $(\hat{\mathbf{h}}_{\mathbf{s}}(i))$ were calculated with a moving average operation over $\hat{\mathbf{h}}(i)$, based on the assumption that human ankle behavior does not change significantly within

a short period of time. In fact, 98% of power in normal human walking is contained below 10 Hz and 99% below 15 Hz [24]. It is also known that the reflex loop delay is greater than 40 ms, which means feedback cannot respond to impulsive inputs within this period [25]–[27]. Thus, a window size (w) for the moving average was set as 40 ms

$$\hat{\mathbf{h}}_{\mathrm{s}}(i) = \frac{1}{N_w} \sum_{j=i-w/2}^{i+w/2} \hat{\mathbf{h}}(j) \tag{6}$$

where N_w is the number of $\hat{\mathbf{h}}(i)$ inside the window between $i - w/2$ and $i + w/2$.

The smoothed IRF estimates $(\hat{\mathbf{h}}_{\mathbf{s}}(i))$ were approximated by a second order model consisting of inertia $(I(i))$, viscosity $(B(i))$, and stiffness $(K(i))$, and its goodness-of-fit was calculated. For each time step i, the best fit parameters $(I^*(i), B^*(i), K^*(i))$ were estimated by minimizing the mean squared error between the IRF of the model $(\mathbf{h}_{\mathbf{model}}(i))$ constructed by $I(i), B(i), K(i)$ and $\hat{\mathbf{h}}_{\mathbf{s}}(i)$. An unconstrained nonlinear optimization method (Nelder-Mead simplex method: MATLAB's *fminsearch* function) [28] was used to find the best fit IRF model $(\mathbf{h}^*_{\mathbf{model}}(i))$. Since the optimal parameters $(I^*(i), B^*(i), K^*(i))$ include contributions from the robot dynamics as well as ankle dynamics, ankle parameters $(I^*_{\mathrm{Ankle}}(i), B^*_{\mathrm{Ankle}}(i), K^*_{\mathrm{Ankle}}(i))$ can be obtained after compensating for Anklebot dynamics in ankle joint coordinates, which also were accurately approximated by a second order system $(I_{\mathrm{Abot}}, B_{\mathrm{Abot}}, K_{\mathrm{Abot}})$ [29]. As impedances add linearly at a common motion connection, and the robot and the ankle shared the same motion in this study, the ankle parameters were calculated as

$$\begin{aligned} I^*_{\mathrm{Ankle}}(i) &= I^*(i) - I_{\mathrm{Abot}} \\ B^*_{\mathrm{Ankle}}(i) &= B^*(i) - B_{\mathrm{Abot}} \\ K^*_{\mathrm{Ankle}}(i) &= K^*(i) - K_{\mathrm{Abot}}. \end{aligned} \tag{7}$$

The reliability of IRF estimation was evaluated by calculating the percentage variance accounted for $(\%VAF)$ between $z_r(i)$ and $\hat{z}_r(i)$ for each realization r (8) and averaged over the entire selected realizations R, where $\hat{z}_r(i)$ was the output predicted by the convolution of $u_r(i)$ and $\hat{\mathbf{h}}_{\mathbf{s}}(i)$. In addition, the reliability of the second order model approximation was calculated in two ways. First, the goodness-of-fit of the model was evaluated from the $\%VAF$ between $\mathbf{h}^*_{\mathbf{model}}(i)$ and $\hat{\mathbf{h}}^*_{\mathbf{model}}(i)$ for each time step i (9) and averaged over the time steps. Second, the $\%VAF$ between $z_r(i)$ and $\hat{z}_{r,model}(i)$ was calculated similarly as (8), where $\hat{z}_{r,model}(i)$ was the output predicted by the convolution of $u_r(i)$ and $\mathbf{h}^*_{\mathbf{model}}$

$$\%VAF_{\mathrm{output}}(r) = 100 \times \left(1 - \frac{\mathrm{var}\left(z_r(i) - \hat{z}_r(i)\right)}{\mathrm{var}\left(z_r(i)\right)}\right) \tag{8}$$

$$\%VAF_{\mathrm{IRF}}(i) = 100! \left(1 - \frac{\mathrm{var}\left(\hat{\mathbf{h}}_{\mathbf{s}}(i) - \mathbf{h}^*_{\boldsymbol{model}}(i)\right)}{\mathrm{var}\left(\hat{\mathbf{h}}_{\mathbf{s}}(i)\right)}\right) \tag{9}$$

$$\%VAF_{\mathrm{output,model}}(r) = 100\left(1 - \frac{\mathrm{var}\left(z_r(i) - \hat{z}_{\mathrm{model,r}}(i)\right)}{\mathrm{var}\left(z_r(i)\right)}\right). \tag{10}$$

E. Ankle Parameters in Subgait Phases and Around Heel-Strike and Toe-Off

IRF estimates and ankle parameters were identified at every 2 ms from pre-swing through swing to early stance. This corresponds to the period when toe and/or heel were off the ground. To clearly see how ankle parameters change across the gait cycle, representative parameter values for each of five subgait phases (pre-swing, initial swing, mid-swing, terminal swing, and early stance) were calculated by averaging identification results within each subphase into single values; early stance begins with heel-strike and ends with toe contact, pre-swing begins with contralateral heel-strike and ends at toe-off, and swing was evenly divided into three periods: initial swing, mid-swing, and terminal swing (Fig. 1).

Ankle parameters around heel-strike and toe-off were more closely examined to track any parameter changes due to the discrete transition between stance and swing. Parameters around heel-strike (HS^- and HS^+ in Fig. 1) were compared with the mean values within a period from the start of terminal swing to 40 ms before heel-strike (TSW^-). Similarly, parameters around toe-off (TO^- and TO^+) were compared with the mean values within a period between the start of pre-swing and 40 ms before toe-off (PSW^-) (Fig. 1).

F. Statistical Analysis

Statistical analyses were performed on the pooled data of all subjects to compare time-varying ankle parameters across five subgait phases from pre-swing to early stance. For each ankle parameter and each direction, one-way ANOVA (MATLAB's *anova1* function) was applied to assess differences between pre-swing and early stance. Tukey's honestly significant difference tests (MATLAB's *multcompare* function) were then used for pairwise comparisons. To determine statistical differences of each ankle parameter in the IE and DP directions, paired t-tests (MATLAB's *ttest2* function) were performed for each subgait phase separately. Furthermore, to test the significance of parameter changes around heel-strike and toe-off, Wilcoxon-rank tests (MATLAB's *signrank* function) were performed. In all statistical analyses, a significance level of 0.05 was used.

III. Results

A. Ensemble Set Construction

All subjects walked on a treadmill at their preferred walking speed for about 15 minutes without any discomfort. Samples of inputs (u_r), output measurements (z_m), outputs due to ankle dynamics (z_r), and corresponding EMG records of a representative subject are shown in Fig. 3.

Subjects' selected preferred walking speed was lower than typical walking speed, possibly due to the added mass of the experimental apparatus. More than 550 realizations were extracted from 13 minutes of perturbed walking for the construction of the stance and swing ensemble sets. All realizations of the stance (or swing) set $(L_{\mathrm{set}}(r))$ were normalized to the mean stance (or swing) duration $(\overline{L}_{\mathrm{set}}(r))$, and the outermost 5% of realizations from the mean were discarded for each set separately. After the normalization process, outlier realizations were further

TABLE I
SUMMARY OF WALKING EXPERIMENT FOR ENSEMBLE SET CONSTRUCTION

	Walking Speed (km/h)	Total Stride Number	Rejection Ratio by 3 Criteria	Stride Duration CV	Stance Duration CV	Swing Duration CV	Distortion Ratio (Stance)	Distortion Ratio (Swing)	Swing/ Stride
Mean	2.8	554.2	0.15	0.025	0.032	0.054	0.023	0.040	0.40
(SD)	(0.4)	(37.4)	(0.02)	(0.007)	(0.010)	(0.014)	(0.007)	(0.011)	(0.03)

The mean and standard deviation (SD) of all subjects are presented.

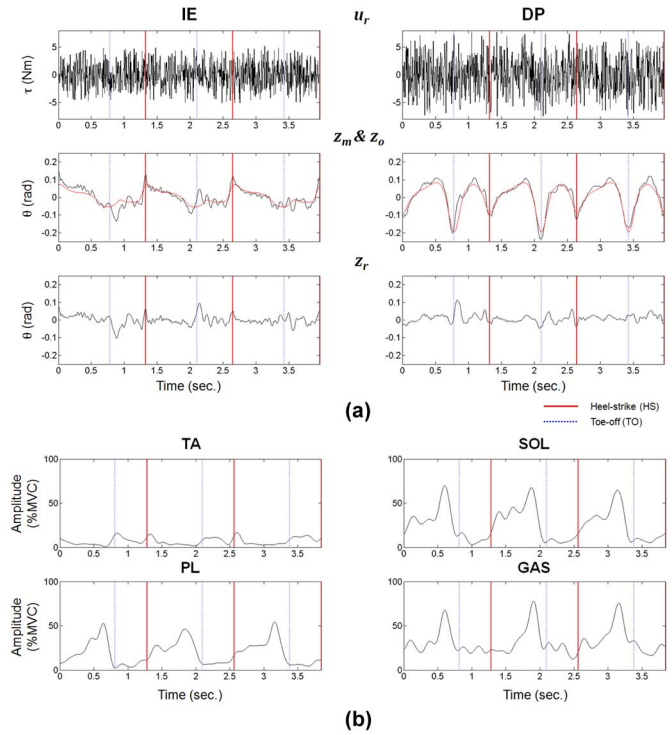

Fig. 3. Sampled inputs, outputs, and EMG records. Samples of three strides of a representative subject are shown. Solid red bars and dotted blue bars represent HS and TO, respectively (a): Torque inputs (u_r), output measurements (z_m, black lines in the second row), nominal ankle trajectories (z_0, red lines in the second row), outputs due to ankle dynamics (z_r). Left column: IE direction, right column: DP direction. (b): Normalized EMG amplitudes (%MVC) of all measured muscles.

rejected according to the spatial and neurophysiological criteria explained in Section II. About 15% of all realizations were discarded based on the three rejection criteria. The distortion ratio due to the normalization process (time-scaling) was calculated based on selected realizations as

$$\text{distortion ratio}_{\text{set}} = \frac{1}{R}\sum_{r=1}^{R}\left|\frac{L_{\text{set}}(r)-\overline{L}_{\text{set}}}{\overline{L}_{\text{set}}}\right|. \qquad (11)$$

The distortion ratio was small: less than 3% and 4% for stance and swing, respectively. The number of realizations for the normalized ensemble sets was more than 450, and the corresponding coefficient of variation (CV) for each set was small: 0.032 and 0.054 for stance and swing, respectively (Table I). This large number of repetitions with reduced variability supported the use of the ensemble-based approach.

B. Time-Varying Ankle Parameters in Subgait Phases

Applications of the modified LTV ensemble-based system identification on u_r and z_r enabled estimation of IRF ($\hat{\mathbf{h}}$) and smoothed IRF ($\hat{\mathbf{h}}_\mathbf{s}$) in joint coordinates. The reliability of system identification was high; the $\%VAF_{\text{output}}$ was 87.6% and 89.7% for IE and DP directions, respectively, when averaged across all subjects (Table II), implying that the estimated ankle dynamics ($\hat{\mathbf{h}}_\mathbf{s}$) accounted for almost 90% of the measured variance. Examples of measured outputs (z_r) and reconstructed outputs ($\hat{z}_r$) are provided in Fig. 4. Furthermore, $\hat{\mathbf{h}}_\mathbf{s}$ was well approximated by a second order system (Fig. 5); the $\%VAF_{\text{IRF}}$ was higher than 90% in all subgait phases and in both DOFs, except during pre-swing in the DP direction (85.6%), and the $\%VAF_{\text{output,model}}$ was 83.6% and 85.7% for IE and DP directions, respectively (Table II).

TABLE II
RELIABILITY MEASURES FOR IRF ESTIMATION AND SECOND ORDER MODEL APPROXIMATION

Reliability Measure / Direction	$\%VAF_{output}$	$\%VAF_{output,model}$	$\%VAF_{IRF}$				
			PSW	ISW	MSW	TSW	EST
IE	87.6 (3.1)	83.6 (3.7)	95.0 (1.5)	96.5 (1.0)	98.7 (0.4)	98.2 (0.9)	92.5 (3.9)
DP	89.7 (2.6)	85.7 (4.5)	85.6 (4.7)	94.1 (4.4)	98.3 (0.6)	97.5 (0.9)	92.0 (4.3)

Mean and SD of all subjects are presented.

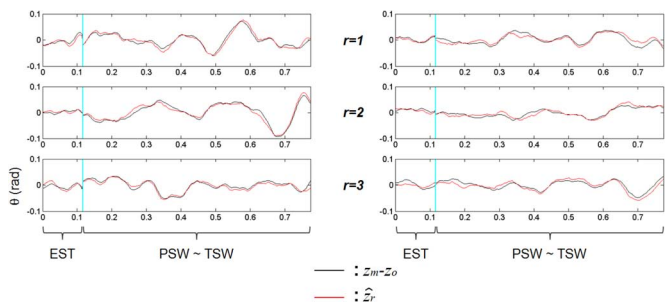

Fig. 4. Samples of outputs due to ankle dynamics (z_r) and reconstructed outputs ($\hat{z}_r$). z_r and $\hat{z}_r$ are represented as black and red lines, respectively. Three realizations of a representative subject are shown. Left column: IE direction, right column: DP direction.

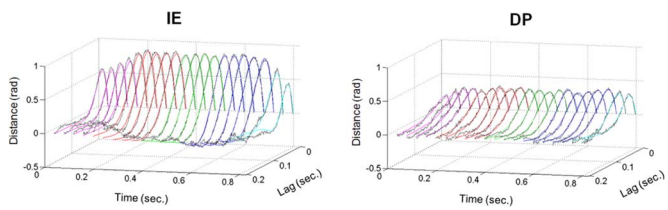

Fig. 5. Representative results of smoothed IRF estimates ($\hat{\mathbf{h}}_s$) and the best second order model approximates ($\mathbf{h}^*_{\mathbf{model}}$). Smoothed IRF estimates ($\hat{\mathbf{h}}_s$) and the best fit second order model approximates ($\mathbf{h}^*_{\mathbf{model}}$) are represented as gray and colored lines (magenta: PSW, red: ISW, green: MSW, blue: TSW, cyan: EST), respectively. The start of PSW is set as zero time, and the time step between estimates is 40 ms. Left column: IE direction, right column: DP direction.

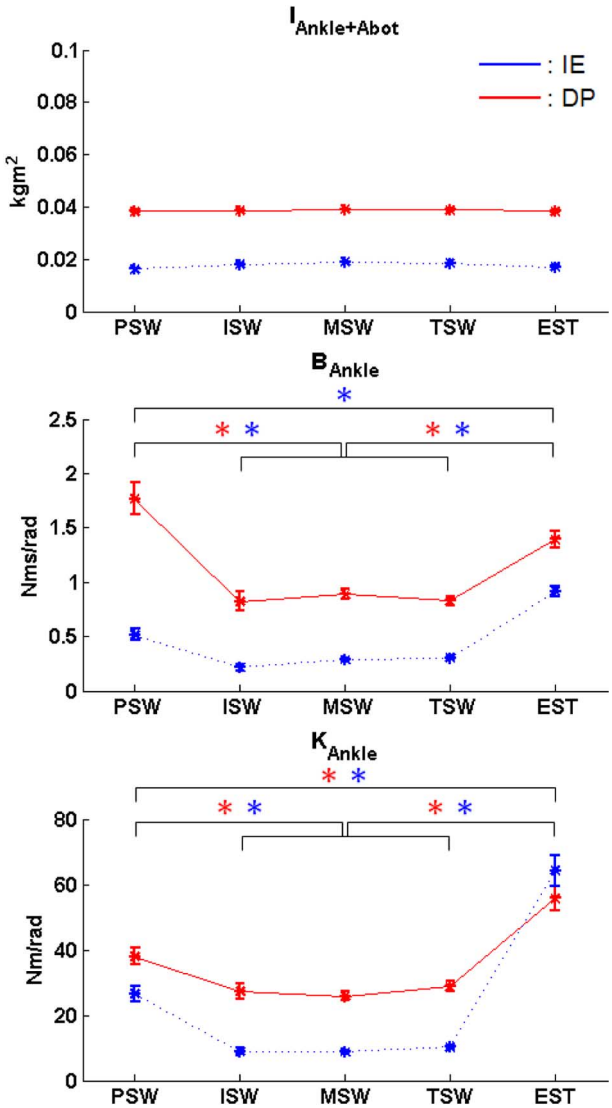

Fig. 6. Time-varying ankle parameters in gait subphases. Representative values for five gait subphases were obtained by averaging results within each gait subphase. Dotted blue lines and solid red lines denote results in IE and DP directions, respectively. Asterisks denote statistical difference ($p < 0.05$). Mean and mean $\pm$ 1 standard error (SE) of all subjects are illustrated as asterisks and bars, respectively.

Ankle parameters in five subphases of gait are shown in Fig. 6. Closed-loop inertia ($I_{\mathrm{Ankle+Abot}}$) was reported since I_{Abot} was a few times greater than I_{Ankle} [30], [31], and even a small estimation error of I_{Abot} may mislead interpretation of time-varying I_{Ankle}. Viscosity and stiffness parameters exhibited clear and consistent time-varying patterns across all subjects, while inertia was much less variable throughout all subgait phases. First, B_{Ankle} and K_{Ankle} were significantly higher in DP than IE in all conditions ($p < 0.001$), except early stance when the stiffness of the two DOFs converged ($p > 0.05$). Second, for both IE and DP, B_{Ankle} and K_{Ankle} significantly decreased ($p < 0.01$) at the end of stance (from pre-swing to initial swing), remained relatively constant across swing ($p > 0.05$), and substantially increased ($p < 0.001$) after heel-strike (from terminal swing to early stance). In addition, B_{Ankle} in IE and K_{Ankle} in both directions were significantly higher in early stance than in pre-swing ($p < 0.001$).

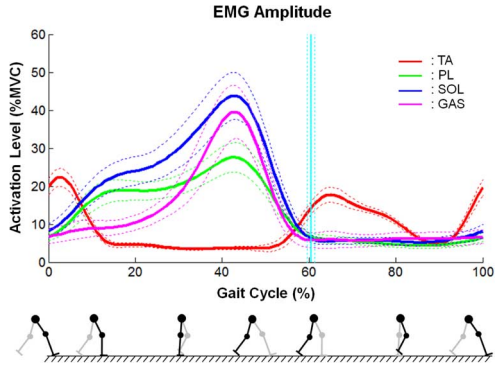

Fig. 7. Normalized EMG amplitude in one gait cycle. The mean (solid lines) and mean $\pm$ 1 SE (dotted lines) of all subjects are illustrated (red: TA, green: PL, blue: SOL, magenta: GAS). Cyan colored vertical line denotes TO mean (solid line) and mean $\pm$ 1 SE (dotted lines).

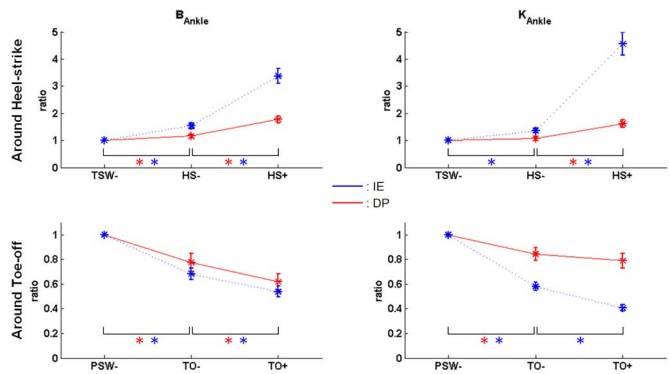

Fig. 8. Ankle parameter changes around HS and TO. Increase ratio of ankle parameters around HS (or TO) in reference to the value in TSW- (or PSW-) was calculated. Dotted blue lines and solid red lines denote results in IE and DP directions, respectively. Asterisks denote statistical difference ($p < 0.05$).

Stereotypical time-varying patterns of ankle parameters were well correlated with EMG profiles across the gait cycle (Fig. 7). In pre-swing, activities of *plantarflexors* (SOL, GAS, and PL) substantially decreased, while TA started to activate before toe-off. *Tibialis* anterior continued to increase up to initial swing, and decreased from initial swing to mid-swing. It increased again in terminal swing before heel-strike. The *plantarflexors* were essentially inactive (5$\sim$10% MVC) across the entire swing phase. After heel-strike, antagonistic muscles in DP (TA and SOL) and IE (TA and PL) were coactivated.

C. Ankle Parameters Around Heel-Strike and Toe-Off

Closer study around heel-strike and toe-off revealed "pre-tuning" of ankle impedance in both DOFs (Fig. 8). More specifically, B_{Ankle} increased at the end of swing before heel-strike ($p < 0.01$) and continued to increase after heel-strike ($p < 0.001$). K_{Ankle} also exhibited the same pattern as B_{Ankle} ($p < 0.001$ in all test conditions except K_{Ankle} in DP at the end of swing ($p > 0.05$)). Although statistical significance was not reached, 8 out of 13 subjects showed increase of K_{Ankle} just before heel-strike. Around toe-off, both B_{Ankle} and K_{Ankle} significantly decreased before toe-off ($p < 0.001$). After toe-off, they further decreased ($p < 0.001$ in all test conditions except K_{Ankle} in DP ($p > 0.05$)).

IV. Discussion

A. Importance of the Study and Reliability of Characterization

Given the significant role of ankle mechanical impedance in interaction with the physical environment, it has been studied over the past few decades. Although much research was conducted in steady-state conditions, little is known about how it is modulated in more general nonstationary conditions, for example during human locomotion. In this study, for the first time (to our knowledge), we investigated time-varying ankle impedance during walking. Our study included heel-strike and toe-off, two key events in the transition from swing to stance or vice versa. Furthermore, extending our previous steady-state studies [15], [17], [31], [32], we characterized ankle impedance in 2 DOFs simultaneously, both in the frontal (IE) and sagittal (DP) planes, again for the first time (to our knowledge).

All subjects who participated in this study could walk on a treadmill with the robot for about 15 minutes with no discomfort. In fact, previous work verified that the effect of unilateral loading due to the experimental setup had minimal effects on spatio-temporal parameters of gait in both overground and treadmill walking conditions [12]. Because of the repetitive and periodic nature of walking, hundreds of realizations could be generated in a relatively short time; 13 minutes of walking with perturbations generated more than 550 strides. Even after outlier rejection the number of realizations was still over 450. This, together with the low variability of the stance and swing ensembles, supported the use of an ensemble-based approach to characterize ankle impedance during walking; the CV for stance and swing durations were 0.032 and 0.054, respectively. The modified LTV ensemble-based system identification methods we used enabled reliable estimation of impulse response functions between pre-swing and early stance ($\%VAF_{\mathrm{output}} > 87\%$ and >89% for IE and DP, respectively), and the best-fit second order models accounted for almost all of the variance of the estimates in all subgait phases in both DOFs, consistent with our previous findings in steady-state dynamic studies [17], [31].

B. Stereotypical Time-Varying Ankle Parameters and Pretuning Behavior

Several consistent and notable time-varying ankle behaviors were observed in both DOFs across all subjects. First, B_{Ankle} and K_{Ankle} significantly decreased from pre-swing to initial swing. This observation was consistent with decreasing activation of *plantarflexors* (SOL, GAS, and PL) from the end of terminal stance to initial swing. Both parameters remained relatively constant throughout the swing phase and substantially increased in early stance.

Close study of heel-strike and toe-off revealed that B_{Ankle} and K_{Ankle} decreased before toe-off. In addition, they started to increase in terminal swing before heel-strike. These "pretuning" behaviors of the ankle may be essential to maintain natural and stable human walking. For example, lowering ankle impedance before toe-off may assist dorsiflexion of the foot to provide toe clearance in initial swing. Increased impedance before heel-strike may prepare for "shock-absorption" in the loading response after heel-strike. In addition to shock absorption, increased ankle impedance during the loading phase exerts a sagittal plane torque on the shank which acts to move the knee from hyperextension to a slightly flexed position appropriate for absorbing the kinetic energy of the descending body mass.

Increased B_{Ankle} and K_{Ankle} in both DOFs in early stance might be attributed to coactivation of antagonistic muscles (TA and PL for IE and TA and SOL for DP) [33]. While this may suffice for the DP direction, the rapid increase of K_{Ankle} in the IE direction to a value comparable to or even exceeding that of the DP direction cannot be explained by coactivation alone. Our previous studies showed that K_{Ankle} in the IE direction was several times lower than in the DP direction even when muscles were active [31], [32]. What might account for the present observations? One possible explanation is that the ankle joint "locks" in the frontal plane right after heel-strike. It has been reported that the subtalar joint, which is responsible for IE movements, locks with eversion when heel-strike occurs [34]. Furthermore, it has been reported that the mortise of the ankle, the space formed by the top of the talus and the lower ends of the tibia and the fibula, locks in the frontal plane at the moment of the heel-strike [35], [36]. Another possible explanation is the stiffness increase due to the compression of soft tissues [37]. Whatever its origin, the substantial increase of frontal plane ankle impedance serves to improve lateral stability from the moment of heel-strike throughout the loading response.

C. Comparison With Previous Work

As described previously, only one study directly measured ankle impedance during walking, and only in the sagittal plane [10]. That study estimated B_{Ankle} and K_{Ankle} in mid-stance and terminal stance, i.e., when the foot was flat on the ground. Both parameters were found to increase progressively throughout the stance phase. B_{Ankle} and K_{Ankle} in terminal stance were substantially higher than those during pre-swing identified in our study ($B_{\mathrm{Ankle}} = 0.038$ Nms/rad/kg, $K_{\mathrm{Ankle}} = 4.6$ Nm/rad/kg), implying a rapid drop of ankle impedance after the contralateral leg hits the ground. In addition, our finding of K_{Ankle} in early stance further extends a linear trend of K_{Ankle} in stance from early stance to terminal stance. No comparison is available for IE, since this previous work was limited to DP.

D. Effect of Time-Scaling on Impedance Estimation

To assess the effect of normalization (time-scaling) on impedance estimation, simple simulations were performed with several second order models having different time varying parameters, covering a range comparable to the results of this study. Estimation errors were calculated for various distortion ratios. As expected, the impedance estimation error increased with the distortion ratio. Nevertheless, it was limited. Based on simulations, the estimation errors for viscosity and stiffness for the time-scaled stance and swing ensembles were expected to be less than 4% and 6%, respectively. A full description of these simulations is provided in [29].

In addition, two sets of ankle parameters, one estimated from time-scaled data and the other from nonscaled data (using the subensemble approach introduced in [38]), were compared around heel-strike and toe-off. We focused on heel-strike and toe-off since these are the transitional events between stance and swing, where errors due to time-scaling may be most

pronounced. Averaged across all subjects, the differences between these two sets were less than 6%, which was statistically insignificant ($p > 0.05$) [29]. Together with the simulation results, this supports our use of normalized ensemble sets for system identification.

E. Effect of Random Perturbations on Muscle Activity

It has been reported that random perturbations influence reflex activity, though the effect varies depending on perturbation properties (amplitude and bandwidth) as well as experimental conditions. One study showed that reflex activity decreased with application of random perturbations under isometric contractions in a supine posture [39], while another study reported that vibratory motions at the ankle may evoke a substantial stretch reflex response [40].

Following the experimental procedure described in Section II, EMG amplitudes of two sets, one with perturbations and the other without perturbations during walking, were compared. The change of muscle activation due to perturbations was less than 0.5% MVC for all four muscles. In short, the effect of random perturbations was minimal.

F. Effect of Interfacial Dynamics

It is important to realize that interfacial dynamics between foot, shoe and ground may affect our ankle impedance identification procedures. First, actuation of the robot may move not only the foot but also the shank and rest of the lower-limb. While it is reasonable to assume that only the foot moves relative to the shank in swing because the foot has much lower inertia than the shank (0.36 kgm^2 when seen at the ankle joint [41] while the ankle inertia is less than 0.01 kgm^2 [30], [31]), that assumption may be less justifiable when the foot contacts the ground. If actuation of the robot moves the shank as well as the ankle, the effective impedance measured at the ankle joint would be significantly influenced by impedance of the shank and more rostral body segments, mostly through their inertia. However, this was not the case since measured inertia was essentially invariant throughout all subgait phases [$p > 0.05$ when results in swing and stance were compared (Fig. 6)]. Thus, the inertia of shank and more rostral body segments was effectively infinite and our assumption that the robot properly moves the ankle is justified.

Second, interfacial dynamics between the foot and ground may contribute to impedance identification. In detail, contact of the foot with the floor may deform the skin and foot and combine its viscoelasticity with the ankle impedance. This effect is expected to be the most pronounced when heel-strike occurs. According to [37], the deformation of the human subcalcaneal fat pad is highly nonlinear, exhibiting a low stiffness under initial loading which rises sharply to about 1000 kN/m when the tissue is compressed under full body weight. Due to kinematics, when transformed to an equivalent rotational stiffness in ankle joint coordinates, this stiffness is essentially in parallel with that of the ankle. Progressive compression and concomitant stiffening of the subcalcaneal fat pad as body weight is accepted following heel contact may contribute to the progressively increasing ankle stiffness which we observed in the EST phase. Whatever its origin, the net effect is to increase the mechanical stability of the ankle joint as body weight is progressively applied.

Third, slippage at the interface of the shoe and the foot and/or around the knee brace is another issue to be addressed. To minimize relative movements of the foot inside the shoe and slippage of the knee brace, the proper size of shoe and knee brace were carefully selected for each subject among nine and five different sizes, respectively, and secured with multiple fasteners as explained in Section II. High reliability of impedance estimation ($\%VAF_{\text{output}}$ close to 90%) based on linear methods indirectly demonstrated that the effect of the slippage (which is almost certainly nonlinear) was not substantial and ankle impedance could be reliably quantified under the given measurement conditions.

G. Implications for Clinical Applications

The demand for rehabilitation services for people with neurological disorders is rapidly increasing with an aging population. For example, about 800 000 Americans experience a new or recurrent stroke each year [42], and according to World Health Organization, 15 million people suffer stroke worldwide yearly [43].

Damage to descending pathways due to neurological disorders causes severe degradation of sensory/motor performance [44]. An impaired ankle joint has significant adverse effects on ambulatory performance. For example, excessive *plantarflexion* ("drop foot") and inversion of the foot following a stroke cause insufficient toe clearance during swing phase and slapping of the foot after heel-strike. These characteristics, in conjunction with inadequate hip and knee flexion, lead to pathological gait that is slower and asymmetrical.

Spasticity, a velocity-dependent resistance to stretch, and/or passive ankle joint stiffness have been thoroughly studied over the past decades to understand underlying mechanisms of pathophysiological behaviors. These studies have shown that impaired ankle characteristics substantially deviate from an unimpaired baseline. Significant alteration of passive ankle stiffness in dorsiflexion and plantarflexion was observed following stroke [45]–[47] and multiple sclerosis [48], [49]. Stroke patients also exhibited higher reflex stiffness in the spastic/paretic ankle compared to the nonparetic side [50], and reflex stiffness of spinal cord injury patients was significantly higher than healthy controls [51]. Although these previous studies provided a quantification of the paretic ankle not available from widely used clinical assessments such as the Modified Ashworth Scale [52], they are still strictly limited to stationary conditions.

For better rehabilitation, it is also important to understand the etiology of the impairment and disability under task relevant functional situations. If the paretic ankle properties can be quantified in functional locomotion, which are typically nonstationary and time-varying, important links between abnormal ankle properties and functional impairment may be revealed. Characterization of time-varying impedance of the impaired ankle with a wearable ankle robot proposed in this study is one possible approach to address this issue. Several previous studies have shown that walking with the Anklebot, both overground and on a treadmill, is feasible for chronic stroke and multiple

sclerosis patients [12], [53]. We may further provide better conditions to study patients; first, a weight support system may be used to relieve the effect of the added mass during treadmill walking; second, the current system identification method can be slightly modified (for example, by adopting the multi-segment algorithm [54]) to substantially reduce the total measurement time. We believe that investigation of the paretic ankle during walking will add unique and invaluable information to existing quantitative measures and ultimately enable better design of rehabilitation protocols to improve patients' functional motor skills.

ACKNOWLEDGMENT

The authors wish to acknowledge valuable assistance from Dr. R. Kearney of McGill University. The authors also would like to thank Dr. H. I. Krebs and Dr. H. Asada of MIT and Dr. D. Sternad of Northeastern University for their constructive comments and suggestions. N. Hogan is a co-inventor of the MIT patents for the robotic devices used in this study. He holds equity positions in Interactive Motion Technologies, Inc., the company that manufactures this type of technology under license to MIT.

REFERENCES

[1] J. Perry, *Gait Analysis: Normal and Pathologic Functions*. Thorofare, NJ, USA: Slack, 1992.

[2] D. A. Winter, "Energy generation and absorption at the ankle and knee during fast, natural, and slow cadences," *Clin. Orthopaedics Related Res.*, no. 175, pp. 147–154, 1983.

[3] R. E. Kearney and I. W. Hunter, "System-identification of human joint dynamics," *Critical Rev. Biomed. Eng.*, vol. 18, no. 1, pp. 55–87, 1990.

[4] P. L. Weiss, R. E. Kearney, and I. W. Hunter, "Position dependence of ankle joint dynamics.1. Passive mechanics," *J. Biomech.*, vol. 19, no. 9, pp. 727–735, 1986.

[5] P. L. Weiss, R. E. Kearney, and I. W. Hunter, "Position dependence of ankle joint dynamics.2. Active mechanics," *J. Biomech.*, vol. 19, no. 9, pp. 737–751, 1986.

[6] M. Lortie and R. E. Kearney, "Identification of physiological systems: Estimation of linear time-varying dynamics with non-white inputs and noisy outputs," *Med. Biological Eng. Comput.*, vol. 39, no. 3, pp. 381–390, 2001.

[7] D. Ludvig, T. S. Visser, H. Giesbrecht, and R. E. Kearney, "Identification of time-varying intrinsic and reflex joint stiffness," *IEEE Trans. Biomed. Eng.*, vol. 58, no. 6, pp. 1715–1723, Jun. 2011.

[8] R. F. Kirsch and R. E. Kearney, "Identification of time varying stiffness dynamics of the human ankle joint during an imposed movement," *Experimental Brain Res.*, vol. 114, no. 1, pp. 71–85, 1997.

[9] J. B. Macneil, R. E. Kearney, and I. W. Hunter, "Identification of time-varying biological-systems from ensemble data," *IEEE Trans. Biomed. Eng.*, vol. 39, no. 12, pp. 1213–1225, Dec. 1992.

[10] E. J. Rouse, L. J. Hargrove, E. J. Perreault, and T. A. Kuiken, "Estimation of human ankle impedance during walking using the perturberator robot," in *Proc. 4th Int. IEEE Biomedical Robotics Biomechatronics Conf.*, Rome, Italy, 2012, pp. 373–378.

[11] E. J. Rouse, R. D. Gregg, L. J. Hargrove, and J. W. Sensinger, "The difference between stiffness and quasi-stiffness in the context of biomechanical modeling," *IEEE Trans. Biomed. Eng.*, vol. 60, no. 2, pp. 562–568, Feb. 2013.

[12] I. Khanna, A. Roy, M. M. Rodgers, H. I. Krebs, R. M. Macko, and L. W. Forrester, "Effects of unilateral robotic limb loading on gait characteristics in subjects with chronic stroke," *J. Neuroeng. Rehabil.*, vol. 7, p. 23, 2010.

[13] A. Roy, H. I. Krebs, D. J. Williams, C. T. Bever, L. W. Forrester, R. M. Macko, and N. Hogan, "Robot-aided neurorehabilitation: A novel robot for ankle rehabilitation," *IEEE Trans. Robot.*, vol. 25, no. 3, pp. 569–582, Mar. 2009.

[14] A. M. Rastgaar, H. Lee, E. M. Ficanha, P. Ho, H. I. Krebs, and N. Hogan, "Multi-directional dynamic mechanical impedance of the human ankle; A key to anthropomorphism in lower extremity assistive robots," in *Neuro-Robotics: From Brain Machine Interfaces to Rehabilitation Robotics*, P. Artemiadis, Ed. New York, NY, USA: Springer, 2014.

[15] H. Lee, P. Ho, M. A. Rastgaar, H. I. Krebs, and N. Hogan, "Multivariable static ankle mechanical impedance with relaxed muscles," *J. Biomech.*, vol. 44, no. 10, pp. 1901–1908, 2011.

[16] J. Montgomery and D. Avers, *Daniels and Worthingham's Muscle Testing: Techniques of Manual Examination*, 8th ed. Philadelphia, PA, USA: Saunders, 2007.

[17] H. Lee, H. I. Krebs, and N. Hogan, "Multivariable dynamic ankle mechanical impedance with relaxed muscles," *IEEE Trans. Neural Syst. Rehabil. Eng.*, vol. 22, no. 6, pp. 1104–1114, Nov. 2014.

[18] Z. Y. Shi and S. S. Law, "Identification of linear time-varying dynamical systems using Hilbert transform and empirical mode decomposition method," *J. Applied Mechanics—Trans. ASME*, vol. 74, no. 2, pp. 223–230, 2007.

[19] D. Piovesan, P. DiZio, and J. R. Lackner, "A new time-frequency approach to estimate single joint upper limb impedance," in *Proc. Annu. Int. Conf. IEEE Eng. in Medicine and Biology Soc.*, 2009, pp. 1282–1285.

[20] R. Zou, H. L. Wang, and K. H. Chon, "A robust time varying identification algorithm using basis functions," *Ann. Biomed. Eng.*, vol. 31, no. 7, pp. 840–853, 2003.

[21] S. Sanyal, S. L. Kukreja, E. J. Perreault, and D. T. Westwick, "Identification of linear time varying systems using basis pursuit," in *Proc. Annu. Int. Conf. IEEE Eng. in Medicine and Biology Soc.*, 2005, pp. 22–25.

[22] H. Gomi and M. Kawato, "Human arm stiffness and equilibrium-point trajectory during multi-joint movement," *Biological Cybern.*, vol. 76, no. 3, pp. 163–171, 1997.

[23] E. Burdet, R. Osu, D. W. Franklin, T. Yoshioka, T. E. Milner, and M. Kawato, "A method for measuring endpoint stiffness during multi-joint arm movements," *J. Biomech.*, vol. 33, no. 12, pp. 1705–1709, 2000.

[24] E. K. Antonsson and R. W. Mann, "The frequency content of gait," *J. Biomech.*, vol. 18, no. 1, pp. 39–47, 1985.

[25] R. E. Kearney, R. B. Stein, and L. Parameswaran, "Identification of intrinsic and reflex contributions to human ankle stiffness dynamics," *IEEE Trans. Biomed. Eng.*, vol. 44, no. 6, pp. 493–504, Jun. 1997.

[26] M. M. Mirbagheri, H. Barbeau, and R. E. Kearney, "Intrinsic and reflex contributions to human ankle stiffness: Variation with activation level and position," *Experimental Brain Res.*, vol. 135, no. 4, pp. 423–436, 2000.

[27] J. Duysens, M. Trippel, G. A. Horstmann, and V. Dietz, "Gating and reversal of reflexes in ankle muscles during human walking," *Experimental Brain Res.*, vol. 82, no. 2, pp. 351–358, 1990.

[28] J. A. Nelder and R. Mead, "A simplex-method for function minimization," *Computer J.*, vol. 7, no. 4, pp. 308–313, 1965.

[29] H. Lee, "Quantitative characterization of multi-variable human ankle mechanical impedance," PhD Thesis, Mechanical Engineering 2013, Massachusetts Institute of Technology (MIT), Cambridge, MA, USA, p. 1–230.

[30] R. E. Kearney, P. L. Weiss, and R. Morier, "System-identification of human ankle dynamics-intersubject variability and intrasubject reliability," *Clin. Biomech.*, vol. 5, no. 4, pp. 205–217, 1990.

[31] H. Lee, H. I. Krebs, and N. Hogan, "Multivariable dynamic ankle mechanical impedance with active muscles," *IEEE Trans. Neural Syst. Rehabil. Eng.*, vol. 22, no. 5, pp. 971–981, Sep. 2014.

[32] H. Lee, P. Ho, M. Rastgaar, H. I. Krebs, and N. Hogan, "Multivariable static ankle mechanical impedance with active muscles," *IEEE Trans. Neural Syst. Rehabil. Eng.*, vol. 22, no. 1, pp. 44–52, Jan. 2014.

[33] N. Hogan, "Adaptive-control of mechanical impedance by coactivation of antagonist muscles," *IEEE Trans. Automat. Contr.*, vol. 29, no. 8, pp. 681–690, Aug. 1984.

[34] A. L. Logan and L. J. Rowe, *The Foot and Ankle: Clinical Applications*. Gaithersburg, MD, USA: Aspen, 1985.

[35] A. Arndt, P. Westblad, I. Winson, T. Hashimoto, and A. Lundberg, "Ankle and subtalar kinematics measured with intracortical pins during the stance phase of walking," *Foot Ankle Int.*, vol. 25, no. 5, pp. 357–364, 2004.

[36] J. Perry, "Anatomy and biomechanics of the hindfoot," *Clin. Orthop. Relat. Res.*, no. 177, pp. 9–15, 1983.

[37] M. B. Bennett and R. F. Ker, "The mechanical properties of the human subcalcaneal fat pad in compression," *J. Anatomy*, vol. 171, pp. 131–138, 1990.

[38] H. Lee and N. Hogan, "Investigation of human ankle mechanical impedance during locomotion using a wearable ankle robot," in *Proc. IEEE Int. Conf. Robotics and Automation*, 2013, pp. 2636–2641.
[39] R. B. Stein and R. E. Kearney, "Nonlinear behavior of muscle reflexes at the human ankle joint," *J. Neurophysiol.*, vol. 73, no. 1, pp. 65–72, 1995.
[40] R. Ritzmann, A. Kramer, M. Gruber, A. Gollhofer, and W. Taube, "EMG activity during whole body vibration: Motion artifacts or stretch reflexes?," *Eur. J. Applied Physiol.*, vol. 110, no. 1, pp. 143–151, 2010.
[41] S. J. Piazza and S. Delp, "The influence of muscles on knee flexion during the swing phase of gait," *J. Biomech.*, vol. 29, no. 6, pp. 723–733, 1996.
[42] A. S. Go, D. Mozaffarian, and V. L. Roger *et al.*, "Heart disease and stroke statistics—2013 update: A report from the American Heart Association," *Circulation*, vol. 127, no. 1, pp. 6–245, 2013.
[43] [Online]. Available: http://www.strokecenter.org/patients/about-stroke/stroke-statistics/
[44] R. T. Katz and W. Z. Rymer, "Spastic hypertonia—Mechanisms and measurement," *Arch. Physical Medicine and Rehabil.*, vol. 70, no. 2, pp. 144–155, 1989.
[45] S. G. Chung, E. van Rey, Z. Q. Bai, E. J. Roth, and L. Q. Zhang, "Biomechanic changes in passive properties of hemiplegic ankles with spastic hypertonia," *Arch. Physical Medicine and Rehabil.*, vol. 85, no. 10, pp. 1638–1646, 2004.
[46] S. G. Chung, E. Van Rey, Z. Q. Bai, W. Z. Rymer, E. J. Roth, and L. Q. Zhang, "Separate quantification of reflex and nonreflex components of spastic hypertonia in chronic hemiparesis," *Arch. Physical Medicine and Rehabil.*, vol. 89, no. 4, pp. 700–710, 2008.
[47] A. Roy, H. I. Krebs, C. T. Bever, L. W. Forrester, R. F. Macko, and N. Hogan, "Measurement of passive ankle stiffness in subjects with chronic hemiparesis using a novel ankle robot," *J. Neurophysiol.*, vol. 105, no. 5, pp. 2132–2149, 2011.
[48] H. Lee, T. Patterson, J. Ahn, D. Klenk, A. Lo, H. I. Krebs, and N. Hogan, "Static ankle impedance in stroke and multiple sclerosis: A feasibility study," in *Proc. Annu. Int. Conf. IEEE Engineering in Medicine and Biology Soc.*, 2011, pp. 8523–8526.
[49] T. Sinkjaer, E. Toft, K. Larsen, S. Andreassen, and H. J. Hansen, "Non-reflex and reflex mediated ankle joint stiffness in multiple-sclerosis patients with spasticity," *Muscle Nerve*, vol. 16, no. 1, pp. 69–76, 1993.
[50] M. M. Mirbagheri, L. Alibiglou, M. Thajchayapong, and W. Z. Rymer, "Muscle and reflex changes with varying joint angle in hemiparetic stroke," *J. Neuroeng. Rehabil.*, vol. 5, pp. 1–15, 2008.
[51] M. M. Mirbagheri, H. Barbeau, M. Ladouceur, and R. E. Kearney, "Intrinsic and reflex stiffness in normal and spastic, spinal cord injured subjects," *Exp. Brain Res.*, vol. 141, no. 4, pp. 446–459, 2001.
[52] R. W. Bohannon and M. B. Smith, "Interrater reliability of a modified Ashworth scale of muscle spasticity," *Phys. Therapy*, vol. 67, no. 2, pp. 206–207, 1987.
[53] J. Ahn, T. Patterson, H. Lee, D. Klenk, A. Lo, H. I. Krebs, and N. Hogan, "Feasibility of entrainment with ankle mechanical perturbation to treat locomotor deficit of neurologically impaired patients," in *Proc. Annu. Int. Conf. IEEE Eng. in Medicine and Biology Soc.*, 2011, pp. 7474–7477.
[54] D. Ludvig and E. Perreault, "System identification of physiological systems using short data segments," *IEEE Trans. Biomed. Eng.*, vol. 59, no. 12, pp. 3541–3549, Dec. 2012.

Hyunglae Lee (M'13) received the B.S. (*summa cum laude*) and M.S. degrees in mechanical engineering from Seoul National University, Seoul, in 2002 and 2004, respectively, and the Ph.D. degree in mechanical engineering from Massachusetts Institute of Technology (MIT), Cambridge, MA, USA, in 2013.

He worked at Korea Institute of Science and Technology (KIST) (2006 through 2008) and LG Electronics (2004 through 2006) as a Researcher in the field of human-computer interaction, human-robot interaction, and mechanical design. He is currently a Postdoctoral Fellow at the Sensory Motor Performance Program (SMPP), Rehabilitation Institute of Chicago (RIC), Chicago, IL, USA. His current research interests include system identification, rehabilitation robotics, biomechanics, and neuromotor control.

Dr. Lee is a recipient of a Samsung Scholarship and has been awarded the 2014 Sarah Baskin Award for Excellence in Research (1st place) from RIC.

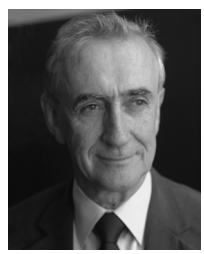

Neville Hogan received the Dip. Eng. (with distinction) from Dublin Institute of Technology, Dublin, Ireland, and the M.S., M.E., and Ph.D. degrees from Massachusetts Institute of Technology (MIT), Cambridge, MA, USA.

He is the Sun Jae Professor of mechanical engineering and a Professor of brain and cognitive sciences at MIT. Following industrial experience in engineering design, he joined MIT's school of Engineering faculty in 1979 and has served as Head and Associate Head of the Mechanical Engineering Department's System Dynamics and Control Division. He is Director of the Newman Laboratory for Biomechanics and Human Rehabilitation and a Founder and Director of Interactive Motion Technologies, Inc. His research interests include robotics, motor neuroscience, and rehabilitation engineering, emphasizing the control of physical contact and dynamic interaction.

Dr. Hogan has been awarded Honorary Doctorates from Delft University of Technology and Dublin Institute of Technology; the Silver Medal of the Royal Academy of Medicine in Ireland; the Henry M. Paynter Outstanding Investigator Award and the Rufus T. Oldenburger Medal from the Dynamic Systems and Control Division of the American Society of Mechanical Engineers.